

# Dark Photon mediated Inelastic Dark Matter in Cosmology, Astrophysics and Colliders

---

Abhishek Roy,<sup>a,b</sup> Prasenjit Sanyal,<sup>a,b</sup> Stefano Scopel,<sup>a,b</sup>

<sup>a</sup>Center for Quantum Spacetime, Sogang University, Seoul 121-742, South Korea

<sup>b</sup>Department of Physics, Sogang University, Seoul 121-742, South Korea

E-mail: [abhishek@sogang.ac.kr](mailto:abhishek@sogang.ac.kr), [prasenjit.sanyal01@gmail.com](mailto:prasenjit.sanyal01@gmail.com),  
[scopel@sogang.ac.kr](mailto:scopel@sogang.ac.kr)

**ABSTRACT:** We provide a systematic discussion of the phenomenology of the Dark Photon iDM ( $A'$ iDM) model, one of the simplest and more straightforward realization of the iDM scenario where the Standard Model is extended by a dark sector containing an additional  $U(1)_D$  gauge symmetry under which all SM particles are neutral, and that couples to the SM hypercharge gauge boson through a kinetic mixing parameter  $\epsilon$ . The model contains two Majorana states  $\chi_1$  and  $\chi_2$  with  $\delta = M_{\chi_2} - M_{\chi_1} > 0$  and  $\chi_1$  the dark matter candidate, and a dark photon  $A'$  with mass  $M_{A'}$ . Our analysis represents an integration of existing ones, where only specific benchmarks of the  $A'$ iDM scenario have been discussed. In particular, we fix the  $U(1)_D$  coupling  $\alpha_D$  equal to the electromagnetic one  $\alpha_{EM}$  and  $\epsilon$  to its experimental upper bound, and perform a complete scan of the remaining parameters  $(M_{\chi_1}, \delta, M_{A'})$ , discussing the  $\chi_1$  relic abundance, its direct and indirect searches, as well as potential signals from astrophysics and accelerators. Our systematic scan shows that  $\alpha_D = \alpha_{EM}$  is not phenomenologically disfavored, as some previous analyses, limited to specific benchmarks, may suggest. We also find that when the  $\chi_1$  relic density matches observation direct and indirect searches are not kinematically accessible. On the other hand we find that the projected luminosity of FASER, a detector searching for Long Lived Particles (LLP) decay at the LHC, can probe or rule out the parameters space of the model for  $M_{\chi_1} \lesssim 7$  GeV,  $100$  MeV  $\lesssim \delta \lesssim 300$  MeV and  $M_{A'} \lesssim 25$  GeV. This range of parameter could be significantly extended by the FASER 2 upgrade proposed for the High-Luminosity phase at the LHC. The parameter space probed by LLP searches at accelerators partially overlaps with that probed by  $\chi_1$  capture in neutron stars. The process is expected to heat-up a neutron star close to the Earth to  $\simeq 2000$  Kelvin providing a potential, albeit challenging, way to detect the Dark Photon iDM scenario in future observations with infrared telescopes.

**KEYWORDS:** Beyond the Standard Model, Particle Nature of Dark Matter, Dark Matter at Colliders, Neutron star kinetic heating

---

## Contents

|          |  |           |
|----------|--|-----------|
| <b>1</b> | <b>Introduction</b>                          | <b>1</b>  |
| <b>2</b> | <b>The Model</b>                             | <b>3</b>  |
| <b>3</b> | <b>Existing Constraints</b>                  | <b>4</b>  |
| 3.1      | Collider Constraints                         | 5         |
| 3.2      | Dark Matter Observables Constraints          | 5         |
| <b>4</b> | <b>Dark Matter capture in Neutron Stars</b>  | <b>7</b>  |
| <b>5</b> | <b>Collider Prospects: FASER and FASER 2</b> | <b>10</b> |
| 5.1      | Analysis and Results                         | 11        |
| <b>6</b> | <b>Discussion and Conclusions</b>            | <b>13</b> |
| <b>A</b> | <b>Decay widths and Lorentz boost</b>        | <b>14</b> |

---

## 1 Introduction

The search for Weakly Interacting Massive Particles (WIMPs), the most natural candidates to provide the Cold Dark Matter that is supposed to have triggered galaxy formation and is believed to provide about 25% of the density of the Universe under an invisible form [1], has proved elusive so far. The increasingly stringent experimental limits puts growing tension on the standard thermal decoupling scenario, which requires a minimal size for the WIMP couplings with SM particles in the early Universe in order to yield the correct value for the relic density. This motivates the interest toward scenarios where WIMPs interact with SM particles comparatively faster in the early Universe than in today DM searches.

An example of such scenarios is inelastic dark matter (iDM), which was first proposed to explain the DAMA anomaly in the context of dark matter direct detection (DD) searches [2]. In this class of models a Dark Matter (DM) particle  $\chi_1$  of mass  $M_{\chi_1}$  interacts with atomic nuclei exclusively by upscattering to a second heavier state  $\chi_2$  with mass  $M_{\chi_2} = M_{\chi_1} + \delta$ . A peculiar feature of iDM is that there is a minimal WIMP incoming speed in the target frame matching the kinematic threshold for inelastic upscattering events and given by:

$$v_{T*} = \sqrt{\frac{2\delta}{\mu_{\chi T}}}, \quad (1.1)$$

with  $\mu_{\chi T}$  the WIMP–target reduced mass. In particular, the WIMPs in our Galaxy are much slower than in the early Universe, so that such velocity-dependent threshold can

suppress the signals in DD searches and at the same time allow for a large-enough WIMP annihilation rate at the time of the WIMP decoupling from the thermal bath to yield the observed relic abundance. Moreover, if at the present time all the  $\chi_2$  heavy states have decayed away, the  $\chi_1\chi_2$  annihilation process in the halo of our Galaxy is not possible and the  $\chi_1\chi_1$  can be suppressed, explaining why also indirect searches have proved ineffective so far.

In order to observe the iDM scenario in today’s Universe the  $\chi_1$  particles need to be accelerated beyond the kinematic threshold. The heavy state  $\chi_2$  can be easily produced in accelerators, where the iDM kinematic threshold is negligible [3–9]. In such case, depending on the value of  $\delta$ , the decay of the  $\chi_2$  particle can be observed at the Large Hadron Collider (LHC) through a displaced vertex either inside the the detector (for example in CMS, ATLAS and LHCb) or in dedicated detectors positioned at some distance away from the interaction points (for example, FASER [10–14], MATHUSLA [15–17], CODEX-b [18–20], AL3X [21], MAPP [22], ANUBIS [23] and FACET [24]). In particular, among the latter only FASER is currently operating in the LHC Run 3 data taking period. In the following we will henceforth restrict our study to FASER and its proposed upgrade FASER 2 for the High-Luminosity phase of the LHC (HL-LHC).

Moreover, the velocity threshold induced by the mass splitting can be overcome when the  $\chi_1$  particles are accelerated by the gravitational potential of a celestial body before up-scattering to the  $\chi_2$  state off the nuclei inside it. If the DM particle is captured inside the star this can lead to detectable astrophysical signals [25–33].

One of the simplest and more straightforward realization of the iDM scenario is in the Dark Photon model (hereafter referred to as  $A'$ iDM). The dark photon is a portal between the SM and dark-sector states [4, 7, 8, 34, 35] that represents a well-motivated framework to circumvent longstanding constraints on dark matter masses below the weak scale, such as the  $Z$  invisible decay limits [36, 37] or the Lee-Weinberg bound [38] (which excludes thermal relics below  $\mathcal{O}(1)$  GeV). In the  $A'$ iDM scenario the Standard Model is extended by a dark sector containing an additional  $U(1)_D$  gauge symmetry (under which all SM particles are neutral and that couples to the SM hypercharge gauge boson through kinetic mixing), and a Dirac fermion which splits into the two Majorana states  $\chi_1$  and  $\chi_2$  [39].

In spite of its simplicity and of the limited number of its free parameters [40], a systematic discussion of the phenomenology of  $A'$ iDM is still lacking in the literature, were it has been only discussed in specific benchmarks [3–9, 41]. The goal of the present paper is to fill this gap by exploring the Dark Photon iDM scenario in a systematic way, combining its relic abundance, DD and indirect detection as well as potential signals from astrophysics and from accelerators. In particular, in our scan we will fix the  $U(1)_D$  coupling equal to the electromagnetic one, showing that this is not phenomenologically disfavored, as one could conclude from analyses that can be found in the literature that are limited to specific benchmarks [41].

The plan of the paper is the following. We outline the  $A'$ iDM scenario in Section 2; in Section 3 we discuss various existing constraints on the model (namely from colliders in Section 3.1 and from the relic density and BBN in Section 3.2); in Section 4 we discuss the potential signal from Neutron Stars (NS); in Section 5 we discuss how the model can be

tested in accelerators. Finally, we provide our discussion and conclusions in Section 6.

## 2 The Model

We consider the simple extension of the standard model (SM) symmetry with an additional  $U(1)_D$  gauge symmetry, whose associated gauge boson is referred to as the dark photon,  $A'$ . The dark photon couples to the SM hypercharge gauge boson through kinetic mixing, which can be expressed as [42, 43],

$$\mathcal{L}_{int} \supset \frac{\epsilon}{2 \cos \theta_W} A'^{\mu\nu} B_{\mu\nu}, \quad (2.1)$$

where  $A'^{\mu\nu}$  and  $B^{\mu\nu}$  are the field strength tensors associated with the  $U(1)_D$  and SM  $U(1)_Y$  gauge groups,  $\cos \theta_W$  is the cosine of weak mixing angle and  $\epsilon \sim \frac{e_D e}{16\pi^2} \ll 1$  parametrizes the strength of the kinetic mixing, with  $e_D$  and  $e$  denoting the  $U(1)_D$  gauge and electromagnetic couplings respectively. The kinetic mixing can be thought to arise radiatively from particles in the loop that are charged under both  $U(1)$  groups. Furthermore, in our analysis we will consider a dark photon with non-vanishing mass  $M_{A'}$ , but will remain agnostic about the mechanism of its generation. The most plausible scenario involves a scalar degree of freedom breaking the  $U(1)_D$  symmetry spontaneously, thereby giving rise to the dark photon's mass while being decoupled from the theory. The dark photon interacts with SM fermions through,

$$\mathcal{L}_{int} = \sum_f \epsilon (C_{A'ff}^V \bar{f} \gamma^\mu f + C_{A'ff}^A \bar{f} \gamma^\mu \gamma_5 f). \quad (2.2)$$

In particular, when  $M_{A'} \lesssim M_Z$  the axial coupling is negligible compared to the vector coupling, and the latter is given by<sup>1</sup> [45],

$$C_{A'ff}^V \approx -\frac{\epsilon}{\cos \theta_W} \frac{M_Z^2 \cos \theta_W e Q_f - M_{A'}^2 g Y_f}{M_Z^2 - M_{A'}^2}, \quad (2.3)$$

where  $Y_f$  corresponds to the hypercharge of the SM fermion.

In this work, we consider an inelastic dark matter (iDM) scenario in which a Dirac fermion  $\chi$  charged under  $U(1)_D$  and described by the following Lagrangian [39]:

$$\mathcal{L}_{int} \supset \bar{\chi} i \gamma^\mu (\partial_\mu + i g_D A'_\mu) \chi - M_\chi \bar{\chi} \chi - \frac{1}{2} M_L (\bar{\chi}^c P_L \chi + h.c) - \frac{1}{2} M_R (\bar{\chi}^c P_R \chi + h.c), \quad (2.4)$$

splits into two nearly degenerate Majorana states  $\chi_{1,2}$  via the Majorana mass terms  $M_{L,R}$  with  $M_\chi \gg M_{L,R}$ . In the mass eigenstate basis the  $A'$ iDM Lagrangian (2.4) can then be

<sup>1</sup>When  $M_{A'} \ll M_Z$  Eq. (2.2) reduces to  $\mathcal{L}_{int} = \epsilon e \sum_f Q_f \bar{f} \gamma^\mu f$ . For our numerical analysis we use for  $C_{A'ff}^V$  the general expression presented in Ref. [4, 44].

| Parameter          | Scanned range             |
|--------------------|---------------------------|
| $M_{\chi_1}$ [GeV] | [1 , 30]                  |
| $\delta$ [GeV]     | $[10^{-4} , 20]$          |
| $M_{A'}$ [GeV]     | [10 , 60]                 |
| $\epsilon$         | $\epsilon_{\max}(M_{A'})$ |
| $\alpha_D$         | $\alpha_{EM}$             |

**Table 1.** Input parameters used in the numerical scan to find the allowed parameter space. Note that  $\epsilon$  is fixed to the maximum allowed value from the LEP limit for given  $M_{A'}$  [44, 46], with  $M_{A'} > M_{\chi_1} + M_{\chi_2}$  condition.

expressed as:

$$\begin{aligned}
\mathcal{L}_{int} \supset & \frac{1}{2} \bar{\chi}_1 i \gamma^\mu \partial_\mu \chi_1 - \frac{1}{2} M_{\chi_1} \bar{\chi}_1 \chi_1 \\
& + \frac{1}{2} \bar{\chi}_2 i \gamma^\mu \partial_\mu \chi_2 - \frac{1}{2} M_{\chi_2} \bar{\chi}_2 \chi_2 \\
& + i g_D A'_\mu \bar{\chi}_1 \gamma^\mu \chi_2 + \frac{1}{2} g_D \frac{M_L - M_R}{2M_\chi} A'_\mu (\bar{\chi}_2 \gamma^\mu \gamma^5 \chi_2 - \bar{\chi}_1 \gamma^\mu \gamma^5 \chi_1) \\
& + \mathcal{O}\left(\frac{M^2}{M_\chi^2}\right),
\end{aligned} \tag{2.5}$$

with  $M_{\chi_{2,1}} = M_\chi \pm \frac{1}{2}(M_L + M_R)$  and  $\delta \equiv M_{\chi_2} - M_{\chi_1} = M_L + M_R$  and where the lighter state  $\chi_1$  is odd under the  $\mathcal{Z}_2$  symmetry and a cosmologically stable DM candidate. We can infer from Eq. (2.5) that the diagonal interactions  $A'_\mu \chi_1 \chi_1$  and  $A'_\mu \chi_2 \chi_2$  are suppressed by a factor of  $1/M_\chi$ . Therefore, in our work we will assume that they are negligible, and consider only the off-diagonal  $A'_\mu \chi_1 \chi_2$  interaction. Hence, the phenomenology is determined by the following 5 parameters:

$$M_{A'}, M_{\chi_1}, \delta, \epsilon, \alpha_D (= g_D^2/4\pi), \tag{2.6}$$

where, as already pointed out, we set  $\alpha_D = \alpha_{EM}$ . Moreover, we set  $M_{A'} \leq 60$  GeV in order to avoid the parameter space where  $M_{A'} \rightarrow M_Z$  and the kinetic mixing parameter  $\epsilon$  is strongly constrained by precision studies at LEP [44, 46] and displaced muon jet searches at CMS [47]. We also avoid in our scan the parameter space for which  $M_{\chi_1} + M_{\chi_2} \geq M_{A'}$  where the dark photon only decays in visible particles and  $\epsilon$  is strongly constrained by accelerator bounds [41, 48].

### 3 Existing Constraints

In this Section we provide a list of the constraints from existing collider and DM observable bounds that we apply to the parameter space of the  $A'$ iDM scenario. In particular, for our phenomenological analysis we perform a flat random scan over the free parameters of Eq. (2.6) within the ranges indicated in Table 1. As already pointed out the upper bound  $M_{A'} \leq 60$  GeV is chosen to avoid the peculiar regime  $M_{A'} \rightarrow M_Z$  of maximal mixing between the dark photon and the SM  $Z$  boson.

### 3.1 Collider Constraints

We consider the bound arising from electroweak precision measurements performed at LEP, which excludes  $\epsilon \lesssim \text{few} \times 10^{-2}$  for dark photon masses  $M_{A'} \gtrsim 10 \text{ GeV}$  [44, 46]. The constraint is strongest when the mass of the dark photon is close to that of the  $Z$  boson, and becomes progressively weaker for  $M_{A'} > M_Z$ . For our analysis, we will fix  $\epsilon$  to the maximum value allowed by LEP electroweak precision constraints for a given  $M_{A'}$ , i.e.  $\epsilon = \epsilon_{\text{max}}(M_{A'})$ . Specifically, for  $M_{A'} \lesssim 10 \text{ GeV}$ , monophoton searches at BaBar provide more stringent constraints than LEP, excluding  $\epsilon \gtrsim 10^{-3}$  from the process  $e^+e^- \rightarrow \gamma A' \rightarrow \gamma \chi_1 \chi_2$  using an integrated luminosity of  $53 \text{ fb}^{-1}$  collected at the  $\Upsilon$  resonance [49, 50]. For  $M_{A'} < 1 \text{ GeV}$ ,  $\epsilon$  is subject to stringent constraints from several experiments, such as LSND [51, 52], E137 [53, 54], and others. We refer the readers to Refs. [41, 55–57] for comprehensive reviews of the limits on  $\epsilon$  across different ranges of  $M_{A'}$ . We therefore restrict our analysis to  $M_{A'} \geq 10 \text{ GeV}$  to avoid the low-mass regime with stringent bounds on  $\epsilon$ , and consider only constraints from LEP, taking  $\epsilon_{\text{max}}(M_{A'})$  from the corresponding solid line in Fig. 1 of Ref. [4].

Since  $M_{\chi_2} \gtrsim M_{\chi_1}$ , the heavier state  $\chi_2$  decays into  $\chi_1 \bar{f} f$  mediated by an off-shell  $A'$ . The heavier state  $\chi_2$  can be long-lived for a highly compressed mass spectrum ( $\delta \ll 1$ ), allowing it to decay outside the LHC detector volume, thereby leading to a monojet signature. In this case, the process  $pp \rightarrow A'/Z \rightarrow j + \chi_2 \chi_1$  produces a hard jet recoiling against the invisible  $\chi_2 \chi_1$  pair escaping the detector. We find that in the parameter space of our scenario the production cross-section for this process is suppressed due to the high  $p_T(j) \geq 200 \text{ GeV}$  cut and is one order of magnitude smaller than the ATLAS sensitivity [58]<sup>2</sup>.

The decay of the  $\chi_2$  particle has also been searched for inside LHC detectors. CMS [47] published some bounds searching for displaced muons, missing transverse energy and a jet (DMJ), albeit only in some specific benchmark points. Recasting such bounds in the general parameter space of  $A'$ iDM would require a dedicated full simulation. On general grounds, such searches are sensitive to large values of the  $\delta$  parameter, due to the short required decay length. On the other hand astrophysical signals are more sensitive to low values of  $\delta$  (see Section 4), corresponding to configurations where the distance between the interaction point and the detector is much larger, as for the FASER detector (see Section 5). For this reason we decide to focus on the latter type of searches and postpone a full discussion of DMJ searches for future work.

Additionally, we also enforce the partial decay width of  $Z \rightarrow \chi_1 \chi_2$  to satisfy  $\Gamma_Z^{\text{inv}} \lesssim \mathcal{O}(10^{-3}) \text{ GeV}$  [63], as  $A'$ - $Z$  mixing can modify the  $Z$  decay width for  $M_{A'} > 10 \text{ GeV}$ .

### 3.2 Dark Matter Observables Constraints

As mentioned in Section 2, in our model  $\chi_1$  serves as viable WIMP DM candidate. In the early Universe,  $\chi_1$  thermalizes with the thermal bath, and its number density is diluted primarily through the co-annihilation process, i.e.,  $\chi_1 \chi_2 \rightarrow A', Z \rightarrow \bar{f} f$  and subdominantly by  $\chi_1 \chi_1 \rightarrow \chi_2 \chi_2$  (via  $A'$  exchange), which is phase-space suppressed. The evolution of the

<sup>2</sup>To calculate the relevant monojet cross section we implement the Dark Photon model in Feynrules [59], generate the CalCHEP file [60] and feed it to micrOMEGAs [61, 62].

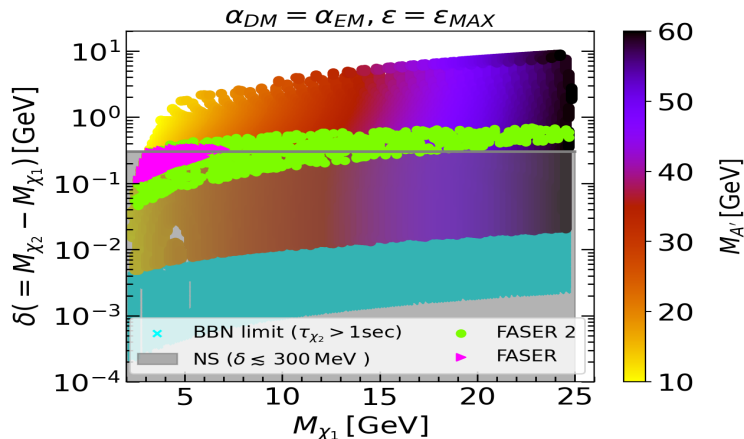


**Figure 1.** Scatter plots in  $M_{\chi_1} - \delta$  plane with color pallets corresponding to  $M_{A'}$ . Note that all the points satisfy collider and DM observables constraints except the cyan colored points, which are disallowed by BBN. The magenta and green areas can be probed by Long Lived Particle searches at FASER and FASER 2 (see Section 5).

number density of DM  $n_{\chi_1}$  is governed by the Boltzmann equation [64, 65],

$$\frac{dn_{\chi_1}}{dt} + 3Hn_{\chi_1} = -\langle\sigma v\rangle_{eff} (n_{\chi_1}^{eq2} - n_{\chi_1}^2), \quad (3.1)$$

where  $n_{\chi_1}^{eq}$  denotes the equilibrium number density of  $\chi_1$ ,  $H$  is the Hubble expansion rate, and  $\langle\sigma v\rangle_{eff}$  represents the DM thermal average effective cross-section, which can be approximated by [4],

$$\langle\sigma v\rangle_{eff} \sim \mathcal{O}(10^{-2}) \left( \frac{\alpha_D}{1/137} \right) \frac{\epsilon_{max}^2(M_{A'}) M_{\chi_1}^2}{M_{A'}^4} e^{-\delta/T}, \quad (3.2)$$

where  $T$  is the temperature of the thermal bath. It is important to highlight that  $\chi_2$  remains in thermal equilibrium as long as the annihilation process  $\chi_2\chi_2 \rightarrow \chi_1\chi_1$  and the decay  $\chi_2 \rightarrow \chi_1\bar{f}f$  do not freeze out. For  $\delta/T \ll 1$ ,  $\chi_1$  and  $\chi_2$  co-annihilate efficiently and the relic abundance is fixed by their simultaneous freeze out. In contrast, for  $\delta/T \gg 1$  the  $\chi_2$  state decouples earlier, leaving  $\chi_1$  without an efficient co-annihilating partner and resulting in a DM relic abundance that exceeds the observed value. To calculate the relic abundance we solve Eq. (3.1) numerically using `micrOMEGAs` [61], which includes all the relevant annihilation and co-annihilation processes. We then impose that the DM relic density falls within the  $2\sigma$  PLANCK interval [1],

$$\Omega_{\chi_1}^{Obs} h^2 = 0.12 \pm 0.0012. \quad (3.3)$$

Since  $\delta/T \ll 1$  from the requirement of the DM relic abundance,  $\chi_2$  can be long-lived due to a compressed mass spectrum between  $\chi_1$  and  $\chi_2$ . The decay of  $\chi_2$  can inject a relativistic degree of freedom to the thermal bath and thereby alter the standard big bang nucleosynthesis (BBN) prediction [66]. To avoid conflict with BBN we impose that the lifetime of  $\chi_2$  satisfies  $\tau_{\chi_2} \lesssim 1.0$  secs.

In Figure 1, we show a scatter plot in the  $M_{\chi_1} - \delta$  plane of the configurations of our scenario whose relic abundance complies with Eq. (3.3). The color pallets correspond to the value of  $M_{A'}$ . Since the  $\chi_1$  decouples from the thermal bath when the temperature drops to approximately  $T \simeq M_{\chi_1}/25$  it follows from Eq. (3.2) that co-annihilation is the dominant process when  $\delta \lesssim 0.04 M_{\chi_1}$  (corresponding to  $\delta/T \simeq 1$  in the exponential). Therefore, we can see that for a given  $M_{\chi_1}$  the upper limit on  $\delta$  increases with  $M_{\chi_1}$ . Furthermore, for a given  $\delta$ ,  $M_{A'}$  increases with increasing  $M_{\chi_1}$  to compensate for the scaling  $M_{\chi_1}^2/M_{A'}^4$  in Eq. (3.2). Fig. 1 also shows that for  $\delta \lesssim 10^{-2}$  GeV the parameter space is ruled out by BBN because  $\tau_{\chi_2} \gtrsim 1.0$  secs. Notice that in Fig. 1 the points extend up to  $M_{\chi_1} \lesssim 25$  GeV because of the  $M_{A'} \lesssim 60$  GeV upper cut in our scan.

The maximum value of  $\delta$  that can be probed by direct detection (DD) experiments corresponds to  $\delta \lesssim 200$  keV [29, 34, 35] and is reached by the heaviest nuclear targets such as xenon, iodine and tungsten when the maximal speed of the WIMPs at the Earth's surface exceeds the kinematic threshold of Eq. (1.1),  $u_{max} > v_{T*}$ , with  $u_{max} \simeq 800$  km/s obtained by combining the WIMP escape velocity in the Galaxy  $u_{esc} \simeq 550$  km/s [67, 68] and the motion of the solar system,  $v_0 \simeq 220$  km/s [69]. On the other hand the elastic process is always negligible, because the relevant loop-mediated cross section is suppressed by the eighth power of  $M_{A'}$  [4] and well below the neutrino floor never exceeding  $10^{-49}$  cm<sup>2</sup>. We conclude that when the relic abundance and the BBN bounds on  $\delta$  are taken into account our model does not produce any signal in DD experiments. Also indirect DM searches, that look for the decay products of DM annihilation in the halo of our Galaxy, cannot detect the  $A'$ iDM scenario. In fact, the  $\chi_1\chi_2$  annihilation process is not available, since at the present time all the  $\chi_2$  particles have decayed away. Moreover, the four-fermion annihilation cross section for the process  $\chi_1\chi_1 \rightarrow A'^*A'^* \rightarrow f\bar{f}f'\bar{f}'$  (mediated by a t-channel  $\chi_2$ ) is velocity suppressed ( $p$ -wave) and negligible [70] at the WIMP speeds in the DM Halo ( $\lesssim 10^{-3}c$ ).

Finally, in our allowed parameter space the co-annihilation process is strongly suppressed at the time of recombination, since  $\delta \gtrsim \mathcal{O}(10^{-2})$  GeV  $\gg T_{rec}$  with  $T_{rec}$  the recombination temperature. As a consequence, also CMB observations [1, 71] do not put any constraint to our scenario.

#### 4 Dark Matter capture in Neutron Stars

The capture process takes place when a  $\chi_1$  particle in the dark halo of our Galaxy crosses a celestial body and, by the same WIMP–nucleus scattering process driving direct detection, loses enough of its energy to become gravitationally captured [72, 73]. This can lead to measurable effects, such as a flux of high-energy neutrinos [74, 75], or an increase in the temperature/luminosity of the celestial body [76]. In the case of inelastic scattering capture extends the kinematic reach of direct detection to larger values of the mass splitting  $\delta$  when the gravitational acceleration of the celestial body drives the  $\chi_1$  particles to higher speeds compared to what happens in terrestrial detectors. In particular, if  $u$  and  $w$  are the speeds of the WIMP far away from the celestial body and at the target position  $r$  inside it, one has

$$w(r)^2 = u^2 + v_{esc}^2(r), \quad (4.1)$$

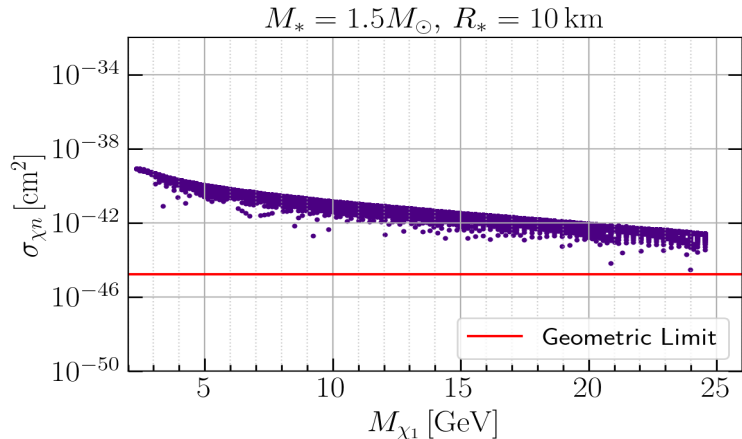


**Figure 2.** Scatter plot in the  $(M_{\chi_1}, \sigma_{\text{inel}})$  plane showing points consistent with relic density, and known experimental constraints. The horizontal line indicates the geometric limit  $\sigma_{\text{geom}}$  for  $M = M_*$  and  $R = R_*$ ; all satisfy  $\sigma_{\text{inel}} > \sigma_{\text{geom}}$ , implying geometric capture saturation.

with  $v_{\text{esc}}(r)$  the escape velocity in the celestial body at  $r$ . This implies that one can have  $w \gg u_{\text{max}}$ , depending on the intensity of the gravitational field. Indeed, at the Earth’s surface the escape velocity is  $\simeq 11 \text{ km/s}$  and  $w \simeq u$ , while that at the center of the Sun  $w$  reaches  $1600 \text{ km/s}$ , allowing to extend the kinematically accessible values of  $\delta$  to  $\simeq 600 \text{ keV}$  [77]. In the case of compact stellar remnants the speed of the scattering WIMP can reach  $\simeq$  a few  $10^4 \text{ km/s}$  for a White Dwarf [28] or a few  $10^5 \text{ km/s}$  for a Neutron Star [31], potentially extending further the values of  $\delta$  that can be probed up to several tens of MeV for the former and hundreds of MeV for the latter. Stellar remnants have the additional advantage that they can be cold enough to potentially detect the anomalous heating produced by the kinetic energy transfer in the scattering process, in absence of the  $\chi_2\chi_1$  coannihilation process and with  $\chi_1\chi_1$  annihilation strongly suppressed. In the following we will discuss the potential signal from  $\chi_1$  capture in a neutron star close to the solar system with representative mass  $M = M_* = 1.5 M_\odot$  and radius  $R = R_* = 10 \text{ km}$ . The gravitational acceleration of such system drives the WIMPs to a maximal speed  $w_{\text{max}} \simeq 0.8c$  corresponding to  $\delta \lesssim 300 \text{ MeV}$  from the kinematic condition (1.1).

The WIMP–nucleon inelastic scattering cross section that drives the capture process is given by [33]:

$$\begin{aligned} \sigma_{\text{inel}} &\simeq \sigma_{\text{el}}\beta_{\text{cl}}, \\ \beta_{\text{cl}} &= \sqrt{1 - \frac{4k\mu_+}{w^2}}, \end{aligned} \quad (4.2)$$

with  $\sigma_{\text{el}}$  the corresponding elastic cross section, that, unless  $M_{A'} \rightarrow M_Z$ , is driven by the vector coupling  $C_{A'\bar{f}f}^V$ . In Eq. (4.2)  $k = \delta/M_{\chi_1}$ ,  $\mu_+ = (1 + \mu)/2$ ,  $\mu = M_{\chi_1}/m_N$  and  $m_N$  is the nucleon mass. The speed of the  $\chi_1$  particles inside the neutron star requires to use the relativistic form for the elastic cross section [33]:

$$\frac{d\sigma_{\text{el}}}{d\cos\theta}(s, t) = \frac{1}{\Lambda^4} \frac{2(\mu^2 + 1)^2 M_{\chi_1}^4 - 4(\mu^2 + 1)\mu^2 s M_{\chi_1}^2 + \mu^4(2s^2 + 2st + t^2)}{16\pi\mu^4 s}, \quad (4.3)$$

with, for a neutron target:

$$\frac{1}{\Lambda^2} = \frac{g_D}{M_{A'}^2} (C_{A'\bar{u}u}^V + 2C_{A'dd}^V). \quad (4.4)$$

Moreover:

$$\begin{aligned} \frac{d\cos\theta}{dt} &= \frac{B\mu^2 + 2\sqrt{B}\mu + B}{M_{\chi_1}^2 \delta t}, \\ t_{\min} &= \frac{M_{\chi_1}^2 \left( B(k^2 + 2k + 2) - \delta t + \sqrt{B}k(k+2)\mu - 2 \right)}{B\mu^2 + 2\sqrt{B}\mu + B}, \\ t_{\max} &= \frac{M_{\chi_1}^2 \left( B(k^2 + 2k + 2) + \delta t + \sqrt{B}k(k+2)\mu - 2 \right)}{B\mu^2 + 2\sqrt{B}\mu + B}, \\ \delta t &= \sqrt{1 - B} \sqrt{B(k^4\mu^2 + 4k^3\mu^2 + 4k^2(\mu^2 - 1) - 8k - 4) - 4\sqrt{B}k(k+2)\mu + 4}, \end{aligned} \quad (4.5)$$

with  $\theta$  the scattering angle in the center of mass,  $s$  and  $t$  the Mandelstam variables,

$$B(M, r) = 1 - \frac{GM}{c^2 r}, \quad (4.6)$$

and  $G$  the gravitational constant.

When the sum of the cross sections of all the neutron targets in the star exceeds the geometrical cross section:

$$\sigma_{\text{geom}} = \frac{\pi R_*^2 m_n}{M}, \quad (4.7)$$

the capture process is optically thick, so that all the  $\chi_1$  particles along the star's path (including the focusing effect of its gravitational attraction) are captured and lose almost all their initial kinetic energy in the celestial body through a large number of scattering processes. In this case, assuming for the WIMPs a Maxwellian distribution with velocity dispersion  $v_{\text{rms}}$ , the capture rate  $C$  (in  $s^{-1}$ ) saturates its geometrical limit:

$$C_* = \frac{\pi R_*^2 (1 - B(M, R))}{v_* B(M, R)} \frac{\rho_{\chi_1}}{m_\chi} \text{Erf} \left( \sqrt{\frac{3}{2}} \frac{v_{\text{rms}}}{v_d} \right) \quad (4.8)$$

with  $v_d = v_0$  if the neutron star is in the solar system and  $\rho_{\chi_1}$  the DM density in the neighborhood of the Sun.

In Fig 2  $\sigma_{\text{inel}}$  is plotted versus  $M_{\chi_1}$  over the full set of configurations that in Fig. 1 yield the correct relic density and are allowed by the BBN limit. In the same plot the horizontal solid line represents the geometrical cross section  $\sigma_{\text{geom}}$  for our benchmark neutron star with  $M = M_*$  and  $R = R_*$ . Such plot shows that  $\sigma_{\text{inel}} > \sigma_{\text{geom}}$  for all the allowed configurations

of the model, so that capture always saturates the geometric value of Eq. (4.8) when it is kinematically possible.

As a consequence, the expected kinetic heating in Kelvin of the neutron star is given by the simple expression [32, 78]:

$$\begin{aligned} T_{\text{kin}} &\simeq \left[ \frac{\rho_{\chi_1}(1-B)B}{4\sigma_{SB}v_{\text{rms}}} \left( \frac{1}{\sqrt{B}} - 1 \right) \text{Erf} \left( \sqrt{\frac{3}{2}} \frac{v_{\text{rms}}}{v_d} \right) \right]^{1/4} \\ &= 1700\text{K} \left( \frac{\rho_{\chi_1}}{0.4\text{GeV cm}^{-3}} \right)^{1/4} F \left( \frac{v_{\text{rms}}}{230\text{km s}^{-1}} \right), \end{aligned} \quad (4.9)$$

where  $\sigma_{SB}$  is the Stefan-Boltzmann constant,  $F(x) = [\text{erf}(x)/(x\text{erf}(1))]^{1/4}$  and, in the second line,  $B = B(M_*, R_*) = 0.55$ ,  $\rho_{\chi_1} \simeq 0.4\text{GeV/cm}^3$  and  $v_{\text{rms}} = \sqrt{3/2}v_0 \simeq 270\text{ km/s}$  (assuming hydrostatic equilibrium in the halo between pressure and gravity [79]). Notice that, provided that the optically thick limit is saturated (i.e. for cross sections exceeding the geometrical limit of Eq. (4.7)) the expected amount of heating is quite insensible to the  $A'$ iDM parameters, including the  $\chi_1$  mass. In an ideal situation a neutron star as old as  $2 \times 10^7$  years [80] could potentially cool down to temperatures below Eq. (4.9), although seizable background heating mechanisms have been discussed in the literature that could prevent this to happen [81, 82]. If in future observations with infrared telescopes such a source could indeed be detected this would in principle allow to probe the full range of configurations of Figs. 1 and 2 using the DM heating effect. In Fig. 1 the region accessible to capture in neutron stars ( $\delta \lesssim 300\text{ MeV}$ ) is delimited by a horizontal solid line.

## 5 Collider Prospects: FASER and FASER 2

At the LHC, the iDM states  $\chi_1$  and  $\chi_2$  are produced via the quark-antiquark annihilation process, i.e. the Drell–Yan process  $pp \rightarrow \chi_1\chi_2$ . In the  $M_{A'} \in [10, 60]\text{ GeV}$  interval considered in our work the corresponding cross section can be approximated by the  $A'$  production cross section multiplied by the branching ratio of  $A' \rightarrow \chi_1\chi_2$  (which in our case is nearly 1) in the narrow-width approximation. The production cross section scales with  $\epsilon^2$  and remains almost independent of  $\alpha_D$  unless  $M_{A'} \rightarrow M_Z$ .

The heavier counterpart  $\chi_2$  is unstable and undergoes a three body decay to  $\chi_1$  and a pair of SM particles through an off-shell  $A'$ , given by  $\chi_2 \rightarrow \chi_1 A'^* \rightarrow \chi_1 f \bar{f}$ . The expression of the relevant decay width  $\Gamma_{\chi_2}$  is given in Appendix A. In particular  $\Gamma_{\chi_2}$  is suppressed at small values of the mass splitting  $\delta$  so that the  $\chi_2$  is a long-lived particle (LLP) on collider scales and its decay products originate from a displaced vertex spatially separated from the primary production point. The proper decay length  $c\tau$  of  $\chi_2$  is given by

$$c\tau = \frac{1.97 \times 10^{-16}}{\Gamma_{\chi_2}} [\text{m}], \quad (5.1)$$

and the decay length in the laboratory (LHC) frame is given by  $\beta\gamma c\tau$ , where  $\tau$  is the life time of  $\chi_2$ ,  $\beta = |\vec{p}/E|$  is the velocity in units of the speed of light  $c$  and  $\gamma = E/M_{\chi_2}$  is the Lorentz

factor in the laboratory frame. Notice that the proper decay length  $c\tau$  depends only on the model parameters. On the other hand, the quantity  $\beta\gamma = |\vec{p}|/M_{\chi_2}$ , which characterizes the Lorentz boost of  $\chi_2$ , is a kinematic variable to be obtained from a numerical simulation.

The currently active ForWard Search ExpeRiment (FASER) [14] is well suited to detect light, weakly interacting LLPs. Such light LLPs typically have small transverse momenta ( $p_T \sim M_{LLP}$ , with  $M_{LLP}$  the LLP mass) and are produced predominantly along the proton–proton collision axis, acquiring a large Lorentz boost in the forward direction. This can be seen in Appendix A where we provide a few examples of boost distributions along the beam axis for a set of selected benchmark points as well as the transverse boost distributions. Specifically, FASER is located 480 m downstream of the proton-proton interaction point used by the ATLAS experiment and is sensitive to LLP decays occurring inside a cylindrical detector volume with radius  $R = 10$  cm and length  $L = 1.5$  m. Additionally, FASER 2 has been proposed as an upgrade of FASER for the High-Luminosity LHC (HL-LHC) phase and as a part of the Forward Physics Facility (FPF) [83, 84]. FASER 2 will be located 620 m downstream of the ATLAS interaction point with a cylindrical decay volume of radius  $R = 1$  m and length  $L = 10$  m, significantly larger than that of FASER.

## 5.1 Analysis and Results

We generated events consisting of Drell-Yan  $pp \rightarrow \chi_1\chi_2$  process followed by the three-body decay  $\chi_2 \rightarrow \chi_1\ell\bar{\ell}$  ( $\ell = e, \mu$ ) using `MadGraph5_aMC@NLO-3.5.10` [85] with `NNPDF31_lo_as_0118` parton distribution function [86], interfaced with an `Universal FeynRules Output (UFO)` [87] model from `FeynRules-2.3` [59]. We calculated the cross sections for a 13.6 TeV center of mass energy and luminosities  $300 \text{ fb}^{-1}$  and  $3000 \text{ fb}^{-1}$  for FASER and FASER 2, respectively. The probability of decay within the detector is given by

$$P_{\text{decay}} = e^{-L_1/\beta\gamma c\tau} - e^{-L_2/\beta\gamma c\tau}, \quad (5.2)$$

where  $L_{1,2}$  are the distances between the LHC interaction point and the points where  $\chi_2$  enters and exists the detector respectively and the decay length in the LHC frame is given by  $\beta\gamma c\tau$ . The probability of decay inside the detector vanishes for those trajectories of  $\chi_2$  which do not intersect the detector. Notice that, according to Eq. (5.2), there is always a finite probability for the  $\chi_2$  to decay inside the detector, even if the characteristic proper decay length  $c\tau$  falls short or exceeds the detector distance. The number of signal events in the detector volume is computed by multiplying the total number of events times the probability of decay of  $\chi_2$  inside the decay volume

$$\mathcal{N}_{\text{signal}} = \mathcal{L}\sigma P_{\text{decay}}\epsilon_{\text{det}}, \quad (5.3)$$

where  $\mathcal{L}$  is the luminosity,  $\sigma$  is the signal cross section and  $\epsilon_{\text{det}}$  is the product of the efficiency for the reconstruction of the events in the detector (which we fix 100% for simplicity) and of the fraction of events passing the energy threshold for the detection of the  $\chi_2$  decay products. In our analysis, following Ref. [10], the latter is fixed by requiring the sum of the energies of the charged tracks to satisfy  $E_{\text{vis}} > 100$  GeV. To compute Eq. (5.3) we generated large samples of  $10^6$  events for each point in the parameter space allowed by the constraints discussed in Sections 3.1 and 3.2.

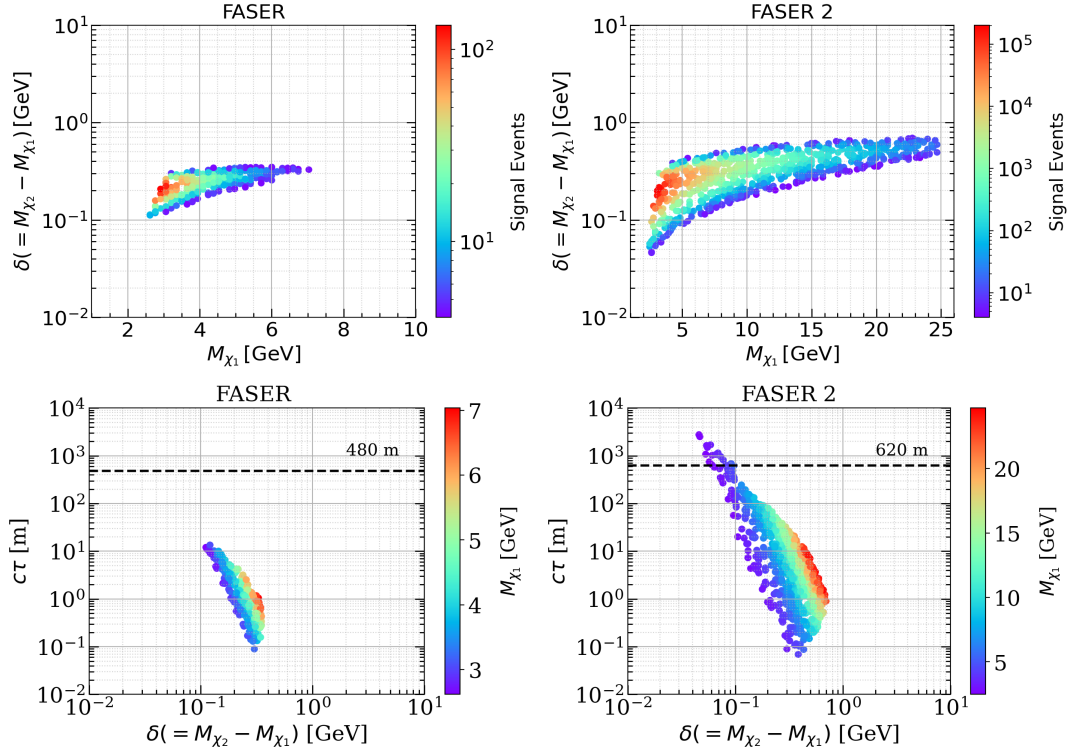


**Figure 3.** Top: Number of signal events in the FASER (left) and FASER 2 (right) decay volumes. Bottom: Range of proper decay length  $c\tau$  for FASER (left) and FASER 2 (right). The horizontal dashed black lines show the distances of FASER (left) and FASER 2 (right) from the ATLAS interaction point.

The results of our simulation is provided in Fig. 3. In the top panel, we show the number of signal events within the decay volumes of FASER and FASER 2. As expected, FASER 2 exhibits both a larger number of signal events and a wider sensitivity reach in the parameter space compared to FASER, owing to its larger decay volume and higher luminosity. In both experiments the number of signal events is larger when  $M_{\chi_1}$  is small due to the larger  $\chi_1\chi_2$  production cross section. FASER is sensitive to mass splitting values in the range  $100 \text{ MeV} \lesssim \delta \lesssim 300 \text{ MeV}$  and to  $\chi_1$  masses up to  $\sim 7 \text{ GeV}$  and  $A'$  masses up to  $\sim 25 \text{ GeV}$ , while for FASER 2 the sensitivity is significantly extended, covering a larger parameter space with  $50 \text{ MeV} \lesssim \delta \lesssim 700 \text{ MeV}$  and  $\chi_1$  masses as large as  $\simeq 25 \text{ GeV}$  and  $A'$  masses up to  $\sim 60 \text{ GeV}$ . In both plots, the blue points along the boundary of the scatter plots correspond to four signal events, which defines the  $2\sigma$  exclusion contours for FASER and FASER 2, assuming a negligible number of background events.

In the lower panel of Fig. 3, we show the range of the proper decay length  $c\tau$  for FASER and FASER 2 corresponding to the scatter plots in the top panel. In particular one can notice that the Lorentz boost and the decay probability of Eq. (5.2) lead to a spread in the values of  $c\tau$ , which is larger in FASER 2 compared to FASER due to its larger decay volume and higher luminosity reach. In the case of FASER  $c\tau$  is smaller than the detector distance, but the large longitudinal boost allows the  $\chi_2$  to decay within the detector volume. On

the other hand, in FASER 2  $c\tau$  can even extend beyond the detector distance. This occurs thanks to a fraction of events with small Lorentz boosts where at low masses of the  $A'$ iDM states the production cross sections is large enough.

The left-hand plot of Fig. 3 shows the parameter space that FASER will probe for its projected luminosity of  $300 \text{ fb}^{-1}$  (in particular, the excluded parameter space assuming no excess is observed).

## 6 Discussion and Conclusions

In the present paper we have provided a systematic discussion of the phenomenology of the Dark Photon iDM ( $A'$ iDM) model, one of the simplest and more straightforward realization of the iDM scenario, for which only specific benchmarks have been discussed in the literature. In this scenario the Standard Model is extended by a dark sector containing an additional  $U(1)_D$  gauge symmetry under which all SM particles are neutral and that couples to the SM hypercharge gauge boson through kinetic mixing. The model contains two Majorana states  $\chi_1$  and  $\chi_2$  that couple to the dark photon  $A'$  with  $\delta = M_{\chi_2} - M_{\chi_1} > 0$  and  $\chi_1$  the dark matter candidate. In particular, in our analysis we have discussed the relic abundance, direct and indirect searches as well as potential signals from astrophysics and accelerators.

The results of our phenomenological analysis are summarized in Fig. 1, where all the points comply with Eq. (3.3), i.e. have relic densities that match observation. Combined with the BBN constraint,  $\tau_{\chi_2} \lesssim 1 \text{ s}$  the cosmologically allowed parameter space corresponds to  $2 \text{ GeV} \lesssim M_{\chi_1} \lesssim 25 \text{ GeV}$ ,  $2 \text{ MeV} \lesssim \delta \lesssim 12 \text{ GeV}$  and  $10 \text{ GeV} \lesssim M_{A'} \lesssim 60 \text{ GeV}$ . In such parameter space the  $\chi_1$  particle is not kinematically accessible to terrestrial Direct Detection experiments. The model is also not accessible to indirect detection from DM annihilation, because the  $\chi_1\chi_2$  annihilation process is not available since in the present Universe all the  $\chi_2$  particles have decayed away, while the  $\chi_1\chi_1$  annihilation process is strongly suppressed. On the other hand we find that the projected luminosity of FASER, a detector searching for Long Lived Particles (LLP) decay at the LHC, can probe or rule out the parameters space of the model for  $M_{\chi_1} \lesssim 7 \text{ GeV}$ ,  $100 \text{ MeV} \lesssim \delta \lesssim 300 \text{ MeV}$  and  $M_{A'} \lesssim 25 \text{ GeV}$ . The parameter space accessible to the LLP search would extend to the full range of  $m_{\chi_1}$  for the FASER 2 upgrade of FASER.

In the full parameter space of the  $A'$ iDM scenario that complies with the relic abundance constraint the WIMP-neutron cross section exceeds the geometrical cross section of a neutron star with mass  $1.5 M_\odot$  and  $R=10 \text{ km}$ . In this regime all the  $\chi_1$  particles that are on the neutron star's path are captured and deposit almost all their kinetic energy in the celestial body through a large number of scattering events. This process is expected to heat-up the neutron star close to the Earth to  $\simeq 2000 \text{ Kelvin}$  if  $\delta \lesssim 300 \text{ MeV}$  (the maximal mass splitting kinematically accessible to the gravitational acceleration of the neutron star). This may provide a potential, albeit challenging, way to detect the Dark Photon iDM scenario in a region of parameter space that partially overlaps with LLP searches at the LHC.

## Acknowledgments

This research was supported by Basic Science Research Program through the National Research Foundation of Korea (NRF) funded by the Ministry of Education through the Center for Quantum Spacetime (CQUeST) of Sogang University with grant number RS-2020-NR049598 and by the Ministry of Science and ICT with grant number RS-2025-24523022. PS would like to thank Felix Kling for useful discussions. PS also acknowledges the KIAS Center for Advanced Computation for providing computing resources. AR would also like to thank Rojalin Padhan for useful discussion.

## A Decay widths and Lorentz boost

For  $M'_A > M_{\chi_1} + M_{\chi_2}$ ,  $A'$  decays to  $\chi_1\chi_2$  by almost 100% and the decay width is given by [88]

$$\begin{aligned} \Gamma(A' \rightarrow \chi_1\chi_2) &= \frac{\alpha_D}{3} M'_A \left(1 - \frac{\delta^2}{M'^2_A}\right)^{3/2} \left(1 + \frac{(M_{\chi_1} + M_{\chi_2})^2}{2M'^2_A}\right) \\ &\times \sqrt{1 - \frac{(M_{\chi_1} + M_{\chi_2})^2}{M'^2_A}}. \end{aligned} \quad (\text{A.1})$$

The three body decay width of  $\chi_2$  to a pair of leptons in the limit  $M'_A \gg M_{\chi_2} > M_{\chi_1}$  is given by [3, 4]

$$\Gamma(\chi_2 \rightarrow \chi_1\ell\bar{\ell}) = \frac{4\epsilon^2\alpha_{EM}\alpha_D\delta^5}{15\pi M'^4_A}. \quad (\text{A.2})$$

The perturbative computation for the hadronic decay mode of  $\chi_2$  applies only when  $\delta \gtrsim 2$  GeV. Therefore, the total decay width of  $\chi_2$  is obtained from the  $\chi_2 \rightarrow \chi_1 e^+ e^-$  process by including the branching ratio (BR) of an off-shell  $A'^*$  decaying into  $e^+ e^-$  pair evaluated at the invariant mass  $M_{ee}^{\text{inv}}$ . Following Refs. [7, 89],  $\Gamma_{\chi_2}$  is given by

$$\begin{aligned} \Gamma_{\chi_2} &= \frac{\epsilon^2\alpha_D\alpha_{EM}}{16\pi^2 M_{\chi_2}^3} \int_{s_2^-}^{s_2^+} ds_2 \int_{s_1^-}^{s_1^+} ds_1 \frac{4|A|^2}{(M_{\chi_1}^2 + M_{\chi_2}^2 + 2M_e^2 - s_1 - s_2 - M_{A'}^2)^2 + M_{A'}^2 \Gamma_{A'}^2} \\ &\times \frac{1}{\text{BR}(M_{A'^*} = M_{ee}^{\text{inv}})}, \end{aligned} \quad (\text{A.3})$$

where  $\Gamma_{A'}$  is the total decay width of  $A'$  and is given in Eq. A.1 and

$$\begin{aligned} |A|^2 &= (s_1 + s_2 - 2M_{\chi_1}M_{\chi_2} - 2M_e^2)[(M_{\chi_1} + M_{\chi_2})^2 + 4M_e^2] + 2(M_e^2 + M_{\chi_1}M_{\chi_2})^2 \\ &- s_1^2 - s_2^2. \end{aligned} \quad (\text{A.4})$$

The integral limits are given by

$$\begin{aligned} s_1^\pm &= M_{\chi_1}^2 + M_e^2 + \frac{1}{2s_2} \left[ (M_{\chi_2}^2 - M_e^2 - s_2)(M_{\chi_1}^2 - M_e^2 + s_2) \right. \\ &\quad \left. \pm \lambda^{1/2}(s_2, M_{\chi_2}^2, M_e^2) \lambda^{1/2}(s_2, M_{\chi_1}^2, M_e^2) \right], \\ s_2^+ &= (M_{\chi_2} - M_e)^2 \quad \text{and} \quad s_2^- = (M_{\chi_1} + M_e)^2, \end{aligned} \quad (\text{A.5})$$

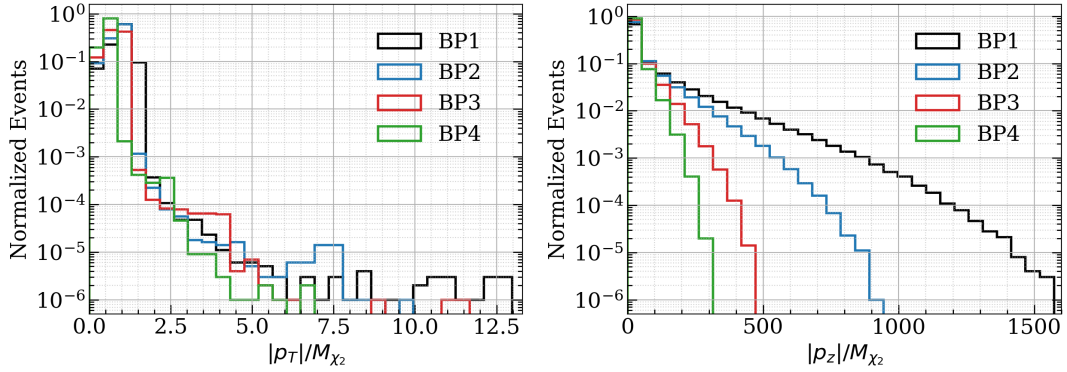


**Figure 4.** Normalized transverse (left) and longitudinal (right) boost distributions for the benchmark points in Eq. (A.8).

where  $\lambda(x, y, z) = (x - y - z)^2 - 4yz$ . To evaluate  $\text{BR}(M_{A'^*} = M_{ee}^{\text{inv}})$  in Eq. A.3, we considered the decay widths of  $A'$  into SM fermions

$$\Gamma(A' \rightarrow f\bar{f}) = N_C \frac{Q_f^2 \epsilon^2 \alpha_{EM}}{3} M_{A'} \left( 1 + 2 \frac{M_f^2}{M_{A'}^2} \right) \sqrt{1 - \frac{4M_f^2}{M_{A'}^2}}, \quad (\text{A.6})$$

where  $N_C = 3$  (1) is the color charge of the quarks (leptons) and  $Q_f$  is the electric charge. For  $M_{A'} \lesssim 2$  GeV, the above perturbative calculation of the  $A' \rightarrow q\bar{q}$  decay width fails [41, 90]. However, in this case the latter can be obtained from the experimentally measured value of  $R_\mu^{\mathcal{H}} = \sigma(e^+e^- \rightarrow \mathcal{H})/\sigma(e^+e^- \rightarrow \mu^+\mu^-)$  [63], such that

$$\Gamma(A' \rightarrow \mathcal{H}) = \Gamma(A' \rightarrow \mu^+\mu^-) R_\mu^{\mathcal{H}}(M_{A'}^2), \quad (\text{A.7})$$

which automatically accounts for the mixing with the QCD vector mesons, the  $\rho$ ,  $\omega$  and  $\phi$ , along with all other non-perturbative QCD effects.

In Eq. 5.2,  $\beta\gamma c\tau$  denotes the decay length of  $\chi_2$  in the laboratory or the LHC frame, where  $\beta\gamma = |\vec{p}|/M_{\chi_2}$  represents the Lorentz boost, which is a purely kinematic quantity. In Fig. 4, we provide examples of the transverse and longitudinal boost distributions for the following benchmark points:

$$\begin{aligned} \text{BP1: } & M_{\chi_1} = 3.35 \text{ GeV}, \quad \delta = 0.21 \text{ GeV}, \quad M_{A'} = 11.60 \text{ GeV}, \\ \text{BP2: } & M_{\chi_1} = 5.56 \text{ GeV}, \quad \delta = 0.32 \text{ GeV}, \quad M_{A'} = 17.62 \text{ GeV}, \\ \text{BP3: } & M_{\chi_1} = 10.71 \text{ GeV}, \quad \delta = 0.27 \text{ GeV}, \quad M_{A'} = 30.45 \text{ GeV}, \\ \text{BP4: } & M_{\chi_1} = 16.15 \text{ GeV}, \quad \delta = 0.56 \text{ GeV}, \quad M_{A'} = 41.68 \text{ GeV}. \end{aligned} \quad (\text{A.8})$$

where we fix  $\alpha_D = \alpha_{EM}$  and  $\epsilon = \epsilon_{\text{max}}(M_{A'})$ . The corresponding values for the proper decay length  $c\tau$ , the production cross section  $\sigma$  of the process  $pp \rightarrow \chi_1\chi_2, \chi_2 \rightarrow \chi_1\ell\ell$  and

the number of signal events in FASER (FASER 2) are given by:

$$\begin{aligned}
\text{BP1: } c\tau &= 0.94 \text{ m, } \sigma = 1332 \text{ pb, } \text{ signal events} = 64 \text{ (138474),} \\
\text{BP2: } c\tau &= 0.57 \text{ m, } \sigma = 549 \text{ pb, } \text{ signal events} = 9 \text{ (14643),} \\
\text{BP3: } c\tau &= 11.32 \text{ m, } \sigma = 139 \text{ pb, } \text{ signal events} = 0 \text{ (228),} \\
\text{BP4: } c\tau &= 0.86 \text{ m, } \sigma = 75 \text{ pb, } \text{ signal events} = 0 \text{ (69).}
\end{aligned}
\tag{A.9}$$

Fig. 4 shows that within the parameter space of interest, the longitudinal or forward boost (right) is significantly larger than the transverse boost (left). It also indicates that the forward boost becomes more pronounced for lower masses of  $\chi_2$ .

## References

- [1] PLANCK collaboration, N. Aghanim et al., *Planck 2018 results. VI. Cosmological parameters*, *Astron. Astrophys.* **641** (2020) A6, [[1807.06209](#)].
- [2] D. Tucker-Smith and N. Weiner, *Inelastic dark matter*, *Phys. Rev. D* **64** (2001) 043502, [[hep-ph/0101138](#)].
- [3] E. Izaguirre, G. Krnjaic and B. Shuve, *Discovering Inelastic Thermal-Relic Dark Matter at Colliders*, *Phys. Rev. D* **93** (2016) 063523, [[1508.03050](#)].
- [4] A. Berlin and F. Kling, *Inelastic Dark Matter at the LHC Lifetime Frontier: ATLAS, CMS, LHCb, CODEX-b, FASER, and MATHUSLA*, *Phys. Rev. D* **99** (2019) 015021, [[1810.01879](#)].
- [5] D. W. Kang, P. Ko and C.-T. Lu, *Exploring properties of long-lived particles in inelastic dark matter models at Belle II*, *JHEP* **04** (2021) 269, [[2101.02503](#)].
- [6] C.-T. Lu, J. Tu and L. Wu, *Probing inelastic dark matter at the LHC, FASER, and STCF*, *Phys. Rev. D* **109** (2024) 015018, [[2309.00271](#)].
- [7] K. Jodłowski, F. Kling, L. Roszkowski and S. Trojanowski, *Extending the reach of FASER, MATHUSLA, and SHiP towards smaller lifetimes using secondary particle production*, *Phys. Rev. D* **101** (2020) 095020, [[1911.11346](#)].
- [8] E. Bertuzzo, A. Scaffidi and M. Taoso, *Searching for inelastic dark matter with future LHC experiments*, *JHEP* **08** (2022) 100, [[2201.12253](#)].
- [9] W. Liu and J. Sun, *Lepton collider imprints of an inelastic dark matter model*, *Phys. Rev. D* **111** (2025) 115022, [[2503.21083](#)].
- [10] J. L. Feng, I. Galon, F. Kling and S. Trojanowski, *ForwArd Search ExpeRiment at the LHC*, *Phys. Rev. D* **97** (2018) 035001, [[1708.09389](#)].
- [11] FASER collaboration, A. Ariga et al., *FASER’s physics reach for long-lived particles*, *Phys. Rev. D* **99** (2019) 095011, [[1811.12522](#)].
- [12] FASER collaboration, A. Ariga et al., *Technical Proposal for FASER: ForwArd Search ExpeRiment at the LHC*, [1812.09139](#).
- [13] FASER collaboration, A. Ariga et al., *FASER: ForwArd Search ExpeRiment at the LHC*, [1901.04468](#).
- [14] FASER collaboration, H. Abreu et al., *The FASER detector*, *JINST* **19** (2024) P05066, [[2207.11427](#)].

- [15] D. Curtin et al., *Long-Lived Particles at the Energy Frontier: The MATHUSLA Physics Case*, *Rept. Prog. Phys.* **82** (2019) 116201, [[1806.07396](#)].
- [16] MATHUSLA collaboration, C. Alpigiani et al., *An Update to the Letter of Intent for MATHUSLA: Search for Long-Lived Particles at the HL-LHC*, [2009.01693](#).
- [17] MATHUSLA collaboration, B. Aitken et al., *MATHUSLA: An External Long-Lived Particle Detector to Maximize the Discovery Potential of the HL-LHC*, [2504.01999](#).
- [18] V. V. Gligorov, S. Knapen, M. Papucci and D. J. Robinson, *Searching for Long-lived Particles: A Compact Detector for Exotics at LHCb*, *Phys. Rev. D* **97** (2018) 015023, [[1708.09395](#)].
- [19] CODEX-B collaboration, G. Aielli et al., *Expression of interest for the CODEX-b detector*, *Eur. Phys. J. C* **80** (2020) 1177, [[1911.00481](#)].
- [20] CODEX-B collaboration, G. Aielli et al., *CODEX-b: Opening New Windows to the Long-Lived Particle Frontier at the LHC: ESPP Update Comprehensive summary*, [2505.05952](#).
- [21] V. V. Gligorov, S. Knapen, B. Nachman, M. Papucci and D. J. Robinson, *Leveraging the ALICE/L3 cavern for long-lived particle searches*, *Phys. Rev. D* **99** (2019) 015023, [[1810.03636](#)].
- [22] J. L. Pinfold, *The MoEDAL experiment: a new light on the high-energy frontier*, *Phil. Trans. Roy. Soc. Lond. A* **377** (2019) 20190382.
- [23] ANUBIS collaboration, O. Brandt et al., *The ANUBIS detector and its sensitivity to neutral long-lived particles*, [2510.26932](#).
- [24] S. Cerci et al., *FACET: A new long-lived particle detector in the very forward region of the CMS experiment*, *JHEP* **06** (2022) 110, [[2201.00019](#)].
- [25] M. McCullough and M. Fairbairn, *Capture of inelastic dark matter in white dwarves*, *Phys. Rev. D* **81** (Apr, 2010) 083520.
- [26] R. Krall and M. Reece, *Last electroweak WIMP standing: pseudo-dirac higgsino status and compact stars as future probes*, *Chinese Physics C* **42** (apr, 2018) 043105.
- [27] D. Hooper, D. Spolyar, A. Vallinotto and N. Y. Gnedin, *Inelastic Dark Matter As An Efficient Fuel For Compact Stars*, *Phys. Rev. D* **81** (2010) 103531, [[1002.0005](#)].
- [28] N. F. Bell, G. Busoni, M. E. Ramirez-Quezada, S. Robles and M. Virgato, *Improved treatment of dark matter capture in white dwarfs*, *JCAP* **10** (2021) 083, [[2104.14367](#)].
- [29] A. Biswas, A. Kar, H. Kim, S. Scopel and L. Velasco-Sevilla, *Improved white dwarves constraints on inelastic dark matter and left-right symmetric models*, *Phys. Rev. D* **106** (2022) 083012, [[2206.06667](#)].
- [30] M. Fujiwara, K. Hamaguchi, N. Nagata and J. Zheng, *Capture of Electroweak Multiplet Dark Matter in Neutron Stars*, [2204.02238](#).
- [31] N. F. Bell, G. Busoni, S. Robles and M. Virgato, *Improved Treatment of Dark Matter Capture in Neutron Stars*, *JCAP* **09** (2020) 028, [[2004.14888](#)].
- [32] N. Raj, P. Tanedo and H.-B. Yu, *Neutron stars at the dark matter direct detection frontier*, *Phys. Rev. D* **97** (Feb, 2018) 043006.
- [33] N. F. Bell, G. Busoni and S. Robles, *Heating up Neutron Stars with Inelastic Dark Matter*, *JCAP* **09** (2018) 018, [[1807.02840](#)].

- [34] D. Tucker-Smith and N. Weiner, *Inelastic dark matter*, *Phys. Rev. D* **64** (2001) 043502, [[hep-ph/0101138](#)].
- [35] D. Tucker-Smith and N. Weiner, *The Status of inelastic dark matter*, *Phys. Rev. D* **72** (2005) 063509, [[hep-ph/0402065](#)].
- [36] J. Kearney, N. Orlofsky and A. Pierce, *Z boson mediated dark matter beyond the effective theory*, *Phys. Rev. D* **95** (2017) 035020, [[1611.05048](#)].
- [37] M. Escudero, A. Berlin, D. Hooper and M.-X. Lin, *Toward (Finally!) Ruling Out Z and Higgs Mediated Dark Matter Models*, *JCAP* **12** (2016) 029, [[1609.09079](#)].
- [38] B. W. Lee and S. Weinberg, *Cosmological Lower Bound on Heavy Neutrino Masses*, *Phys. Rev. Lett.* **39** (1977) 165–168.
- [39] Y. Cui, D. E. Morrissey, D. Poland and L. Randall, *Candidates for Inelastic Dark Matter*, *JHEP* **05** (2009) 076, [[0901.0557](#)].
- [40] E. J. Chun, J.-C. Park and S. Scopel, *Dark matter and a new gauge boson through kinetic mixing*, *JHEP* **02** (2011) 100, [[1011.3300](#)].
- [41] M. Graham, C. Hearty and M. Williams, *Searches for Dark Photons at Accelerators*, *Ann. Rev. Nucl. Part. Sci.* **71** (2021) 37–58, [[2104.10280](#)].
- [42] B. Holdom, *Two U(1)'s and Epsilon Charge Shifts*, *Phys. Lett. B* **166** (1986) 196–198.
- [43] F. del Aguila, G. D. Coughlan and M. Quiros, *Gauge Coupling Renormalization With Several U(1) Factors*, *Nucl. Phys. B* **307** (1988) 633.
- [44] D. Curtin, R. Essig, S. Gori and J. Shelton, *Illuminating Dark Photons with High-Energy Colliders*, *JHEP* **02** (2015) 157, [[1412.0018](#)].
- [45] I. Hoenig, G. Samach and D. Tucker-Smith, *Searching for dilepton resonances below the Z mass at the LHC*, *Phys. Rev. D* **90** (2014) 075016, [[1408.1075](#)].
- [46] A. Hook, E. Izaguirre and J. G. Wacker, *Model Independent Bounds on Kinetic Mixing*, *Adv. High Energy Phys.* **2011** (2011) 859762, [[1006.0973](#)].
- [47] CMS collaboration, A. Hayrapetyan et al., *Search for Inelastic Dark Matter in Events with Two Displaced Muons and Missing Transverse Momentum in Proton-Proton Collisions at  $s=13$  TeV*, *Phys. Rev. Lett.* **132** (2024) 041802, [[2305.11649](#)].
- [48] M. Fabbrichesi, E. Gabrielli and G. Lanfranchi, *The Dark Photon*, [2005.01515](#).
- [49] BABAR collaboration, J. P. Lees et al., *Search for Invisible Decays of a Dark Photon Produced in  $e^+e^-$  Collisions at BaBar*, *Phys. Rev. Lett.* **119** (2017) 131804, [[1702.03327](#)].
- [50] BABAR collaboration, B. Aubert et al., *Search for Invisible Decays of a Light Scalar in Radiative Transitions  $\nu_{3S} \rightarrow \gamma A_0$* , in *34th International Conference on High Energy Physics*, 7, 2008. [0808.0017](#).
- [51] P. deNiverville, M. Pospelov and A. Ritz, *Observing a light dark matter beam with neutrino experiments*, *Phys. Rev. D* **84** (2011) 075020, [[1107.4580](#)].
- [52] LSND collaboration, L. B. Auerbach et al., *Measurement of electron - neutrino - electron elastic scattering*, *Phys. Rev. D* **63** (2001) 112001, [[hep-ex/0101039](#)].
- [53] J. D. Bjorken, S. Ecklund, W. R. Nelson, A. Abashian, C. Church, B. Lu et al., *Search for Neutral Metastable Penetrating Particles Produced in the SLAC Beam Dump*, *Phys. Rev. D* **38** (1988) 3375.

- [54] B. Batell, R. Essig and Z. Surujon, *Strong Constraints on Sub-GeV Dark Sectors from SLAC Beam Dump E137*, *Phys. Rev. Lett.* **113** (2014) 171802, [[1406.2698](#)].
- [55] R. Essig et al., *Working Group Report: New Light Weakly Coupled Particles*, in *Snowmass 2013: Snowmass on the Mississippi*, 10, 2013. [1311.0029](#).
- [56] A. Berlin, S. Gori, P. Schuster and N. Toro, *Dark Sectors at the Fermilab SeaQuest Experiment*, *Phys. Rev. D* **98** (2018) 035011, [[1804.00661](#)].
- [57] E. Izaguirre, Y. Kahn, G. Krnjaic and M. Moschella, *Testing Light Dark Matter Coannihilation With Fixed-Target Experiments*, *Phys. Rev. D* **96** (2017) 055007, [[1703.06881](#)].
- [58] ATLAS collaboration, G. Aad et al., *Search for new phenomena in events with an energetic jet and missing transverse momentum in pp collisions at  $\sqrt{s} = 13$  TeV with the ATLAS detector*, *Phys. Rev. D* **103** (2021) 112006, [[2102.10874](#)].
- [59] A. Alloul, N. D. Christensen, C. Degrande, C. Duhr and B. Fuks, *FeynRules 2.0 - A complete toolbox for tree-level phenomenology*, *Comput. Phys. Commun.* **185** (2014) 2250–2300, [[1310.1921](#)].
- [60] A. Belyaev, N. D. Christensen and A. Pukhov, *CalcHEP 3.4 for collider physics within and beyond the Standard Model*, *Comput. Phys. Commun.* **184** (2013) 1729–1769, [[1207.6082](#)].
- [61] G. Alguero, G. Belanger, F. Boudjema, S. Chakraborti, A. Goudelis, S. Kraml et al., *micrOMEGAs 6.0: N-component dark matter*, *Comput. Phys. Commun.* **299** (2024) 109133, [[2312.14894](#)].
- [62] D. Barducci, G. Belanger, J. Bernon, F. Boudjema, J. Da Silva, S. Kraml et al., *Collider limits on new physics within micrOMEGAs\_4.3*, *Comput. Phys. Commun.* **222** (2018) 327–338, [[1606.03834](#)].
- [63] PARTICLE DATA GROUP collaboration, S. Navas et al., *Review of particle physics*, *Phys. Rev. D* **110** (2024) 030001.
- [64] P. Gondolo and G. Gelmini, *Cosmic abundances of stable particles: Improved analysis*, *Nucl. Phys. B* **360** (1991) 145–179.
- [65] E. W. Kolb and M. S. Turner, *The Early Universe*, vol. 69. Taylor and Francis, 5, 2019, [10.1201/9780429492860](#).
- [66] M. Kawasaki, K. Kohri, T. Moroi and Y. Takaesu, *Revisiting Big-Bang Nucleosynthesis Constraints on Long-Lived Decaying Particles*, *Phys. Rev. D* **97** (2018) 023502, [[1709.01211](#)].
- [67] M. C. Smith et al., *The RAVE Survey: Constraining the Local Galactic Escape Speed*, *Mon. Not. Roy. Astron. Soc.* **379** (2007) 755–772, [[astro-ph/0611671](#)].
- [68] T. Piffl et al., *The RAVE survey: the Galactic escape speed and the mass of the Milky Way*, *Astron. Astrophys.* **562** (2014) A91, [[1309.4293](#)].
- [69] A. M. Green, *Astrophysical uncertainties on direct detection experiments*, *Mod. Phys. Lett. A* **27** (2012) 1230004, [[1112.0524](#)].
- [70] S. J. Clark, B. Dutta and L. E. Strigari, *Dark matter annihilation into four-body final states and implications for the AMS antiproton excess*, *Phys. Rev. D* **97** (Jan, 2018) 023003.
- [71] M. Carrillo González and N. Toro, *Cosmology and signals of light pseudo-Dirac dark matter*, *JHEP* **04** (2022) 060, [[2108.13422](#)].

- [72] A. Gould, *WIMP Distribution in and Evaporation From the Sun*, *Astrophys. J.* **321** (1987) 560.
- [73] A. Gould, *Resonant Enhancements in WIMP Capture by the Earth*, *Astrophys. J.* **321** (1987) 571.
- [74] J. Silk, K. A. Olive and M. Srednicki, *The Photino, the Sun and High-Energy Neutrinos*, *Phys. Rev. Lett.* **55** (1985) 257–259.
- [75] A. Gould, *Resonant Enhancements in WIMP Capture by the Earth*, *Astrophys. J.* **321** (1987) 571.
- [76] I. Goldman and S. Nussinov, *Weakly Interacting Massive Particles and Neutron Stars*, *Phys. Rev. D* **40** (1989) 3221–3230.
- [77] R. Catena and F. Hellström, *New constraints on inelastic dark matter from IceCube*, *JCAP* **10** (2018) 039, [[1808.08082](#)].
- [78] M. Baryakhtar, J. Bramante, S. W. Li, T. Linden and N. Raj, *Dark kinetic heating of neutron stars and an infrared window on wimps, simps, and pure higgsinos*, *Phys. Rev. Lett.* **119** (Sep, 2017) 131801.
- [79] J. D. Lewin and P. F. Smith, *Review of mathematics, numerical factors, and corrections for dark matter experiments based on elastic nuclear recoil*, *Astropart. Phys.* **6** (1996) 87–112.
- [80] D. G. Yakovlev and C. J. Pethick, *Neutron star cooling*, *Ann. Rev. Astron. Astrophys.* **42** (2004) 169–210, [[astro-ph/0402143](#)].
- [81] N. Raj, P. Shivanna and G. N. Rachh, *Exploring reheated sub-40000 kelvin neutron stars with just, elt, and tmt*, *Phys. Rev. D* **109** (Jun, 2024) 123040.
- [82] M. Fujiwara, K. Hamaguchi, N. Nagata and M. E. Ramirez-Quezada, *Vortex creep heating vs. dark matter heating in neutron stars*, *Physics Letters B* **848** (2024) 138341.
- [83] J. L. Feng et al., *The Forward Physics Facility at the High-Luminosity LHC*, *J. Phys. G* **50** (2023) 030501, [[2203.05090](#)].
- [84] J. Adhikary et al., *Scientific program for the Forward Physics Facility*, *Eur. Phys. J. C* **85** (2025) 430, [[2411.04175](#)].
- [85] J. Alwall, M. Herquet, F. Maltoni, O. Mattelaer and T. Stelzer, *MadGraph 5 : Going Beyond*, *JHEP* **06** (2011) 128, [[1106.0522](#)].
- [86] NNPDF collaboration, R. D. Ball et al., *Parton distributions from high-precision collider data*, *Eur. Phys. J. C* **77** (2017) 663, [[1706.00428](#)].
- [87] C. Degrande, C. Duhr, B. Fuks, D. Grellscheid, O. Mattelaer and T. Reiter, *UFO - The Universal FeynRules Output*, *Comput. Phys. Commun.* **183** (2012) 1201–1214, [[1108.2040](#)].
- [88] A. L. Foguel, P. Reimitz and R. Z. Funchal, *Unlocking the inelastic Dark Matter window with vector mediators*, *JHEP* **05** (2025) 001, [[2410.00881](#)].
- [89] G. F. Giudice, D. Kim, J.-C. Park and S. Shin, *Inelastic Boosted Dark Matter at Direct Detection Experiments*, *Phys. Lett. B* **780** (2018) 543–552, [[1712.07126](#)].
- [90] A. L. Foguel, P. Reimitz and R. Z. Funchal, *A robust description of hadronic decays in light vector mediator models*, *JHEP* **04** (2022) 119, [[2201.01788](#)].